Quasisteady aero-acoustic response of orifices

P. Durrieu[a)]
Laboratoire d'Acoustique Université du Maine, URA CNRS 1101, BP 535 Av. O. Messiaen, 72017 Le Mans Cedex, France

G. Hofmans
Applied Physics, CC.2.24, Technische Universiteit Eindhoven, Postbus 513, 5600 MB Eindhoven, The Netherlands

G. Ajello
Laboratoire d'Acoustique Université du Maine, URA CNRS 1101, BP 535 Av. O. Messiaen, 72017 Le Mans Cedex, France

R. Boot
Applied Physics, CC.2.24, Technische Universiteit Eindhoven, Postbus 513, 5600 MB Eindhoven, The Netherlands

Y. Aurégan
Laboratoire d'Acoustique Université du Maine, URA CNRS 1101, BP 535 Av. O. Messiaen, 72017 Le Mans Cedex, France

A. Hirschberg[b)]
Applied Physics, CC.2.24, Technische Universiteit Eindhoven, Postbus 513, 5600 MB Eindhoven, The Netherlands

M. C. A. M. Peters
PULSIM, TNO-TPD, Postbus 155, 2600 AD Delft, The Netherlands

(Received 20 October 1999; revised 18 June 2001; accepted 8 July 2001)

The low frequency response of orifices (slit, circular diaphragm, and perforated plate) in the presence of mean flow is well predicted by a quasisteady theory. A refinement is brought to the theory by considering a Mach number dependent vena contracta coefficient. The measurements of the vena contracta coefficient of a slit agree well with the simple analytical expression existing in the case of the Borda tube orifice. The measured scattering matrix coefficients do not depend strongly on the geometry of the element. If the frequency is increased the moduli remain relatively unaffected while the arguments exhibit a complex behavior which depends on the geometry. From these considerations an anechoic termination efficient at high mass flow is designed. © *2001 Acoustical Society of America.* [DOI: 10.1121/1.1398058]

PACS numbers: 43.28.Py, 43.28.Ra [LCS]

I. INTRODUCTION

Orifices and perforated plates are generic elements in silencers which take care of sound absorption. The quasisteady theory assumes that the acoustic response of such elements can be described as a succession of steady flow states. This approach has been used by, among others, Ingard and Ising,[1] Cummings[2] for orifices, by Ronneberger[3] for sudden expansions in pipe cross sections and grazing flow along wall perforations.[4] A general discussion of engineering applications is provided by Davies.[5] The absorption of sound in such devices has been explained in terms of vortex shedding by Bechert.[6] Bechert[6] showed also that a properly designed orifice placed at the end of a pipe is an anechoic (nonreflecting) termination at a specific Mach number. While more elaborate theories are now available, which describe the frequency dependence of the aero-acoustic response of orifices[7–10] the quasisteady theory remains a most useful design tool. In this paper we provide some information about the frequency range in which this theory is valid. The influence of the orifice geometry (slit, circular hole, and perforated plate) is considered. While we restrict ourselves to low frequencies, relatively high Mach numbers, as found in mufflers, are considered. Finally the theory is applied to design an anechoic termination which has been used in scale experiments of combustion in long pipe-lines.

A simplified model of the steady flow through an orifice placed in a pipe is presented in Fig. 1.

At the orifice, a free jet is formed by separation of the flow. After flow separation the jet contracts from the orifice cross sectional area S_d to a final cross section S_j, the vena contracta. Further downstream the jet flow becomes unstable and a turbulent mixing region is observed before a fully developed pipe flow is recovered. In practice the turbulent mixing region can be quite long, we however assume that all the

[a)]Now at: PSA Peugeot Citroën, Direction Organes, 18, rue des Fauvelles, 92256 La Garenne-Colombes Cedex, France.
[b)]Author to whom correspondence should be addressed; electronic mail: A.Hirschberg@tue.nl

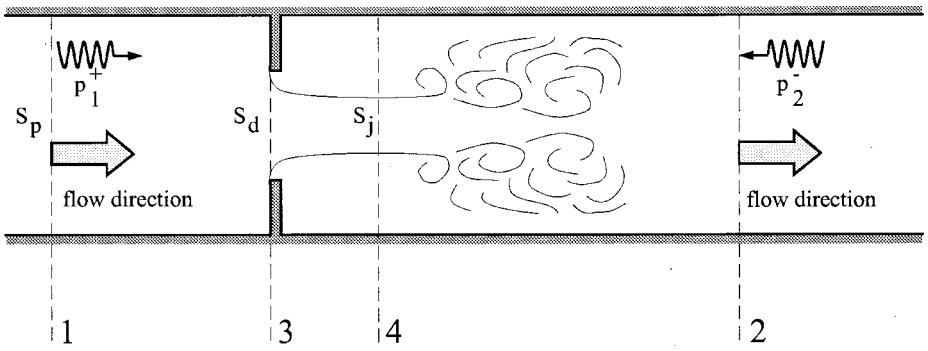

FIG. 1. Harmonic perturbation of a flow passing through a diaphragm. Description of the phenomenon and notations. Regions 1 and 2: one-dimensional flow, region 3: jet formation, region 4: turbulent flow.

relevant acoustical phenomena occur within a few pipe diameters.

A quantitative prediction of the aero-acoustic performance of an orifice involves the knowledge of the ratio S_j/S_d of jet to orifice cross sectional areas, which is called the vena contracta factor Γ_0. Often the theoretical value $\Gamma_0=\pi/(2+\pi)$ for an incompressible flow through a slit shaped orifice in an infinite baffle is quoted. We propose a semiempirical approach allowing us to predict both the effect of compressibility of the flow (Mach number dependency) and of the confinement in the pipe. The key idea is to use an interpolation formula between limit cases which has been derived by Hofmans[10] for the case of a Borda tube orifice (sharp edged pipe segment of cross sectional area S_d placed in the orifice).

The theory is validated by means of scattering matrix measurements obtained by means of a two-load method[11] at the TUE (Technische Universiteit Eindhoven) and TA-HGE (Tenneco Automotive-Heinrich Gillet GmbH & Co. KG) and a two-source method.[11–13] at the LAUM (Laboratoire d'Acoustique de l'Université du Maine).

Finally the design of a robust anechoic pipe termination effective over a broad range of Mach numbers and frequencies is discussed.

II. PREDICTION OF AERO-ACOUSTICAL RESPONSE

A. Wave propagation

Consider a diaphragm as a discontinuity between two uniform pipe segments of cross sectional area S_p. The flow upstream of the discontinuity is assumed to be one-dimensional and is determined by the flow velocity u_1, the pressure p_1, and the density ρ_1. This flow is assumed to be isentropic, there are no incoming fluctuations of the entropy convected with the flow. Downstream of the discontinuity, we assume again a one-dimensional flow with velocity u_2, pressure p_2, and density ρ_2. This flow is assumed to be adiabatic but not isentropic. The modulation of the dissipation in the turbulent mixing region downstream of the jet (see Fig. 1) induces fluctuations in the entropy.

The flow is perturbed by incident acoustic waves p_1^+ and p_2^- corresponding to a wave travelling in the downstream direction at the upstream side and a wave travelling upstream at the downstream side. These perturbations generate acoustic waves p_1^- and p_2^+ travelling upstream at the upstream side and downstream at the downstream side. The pressure perturbations travel with the local speed of sound c_i ($i=1,2$). The entropy perturbation σ_2' is convected with the flow velocity u_2.

The present discussion is further restricted to harmonic perturbations of radial frequency ω. The sign convention $\exp[i\omega t]$ is used. The amplitude of the perturbations are indicated by a prime. We furthermore neglect sound production by the discontinuity which is not correlated with the incoming perturbations. In such a case the pressure waves generated at the discontinuity can be expressed in terms of the scattering matrix:

$$\begin{pmatrix} p_2^+ \\ p_1^- \end{pmatrix} = \begin{pmatrix} t^+ & r^- \\ r^+ & t^- \end{pmatrix} \begin{pmatrix} p_1^+ \\ p_2^- \end{pmatrix}. \tag{1}$$

The elements t^+ and r^+ are the transmission and reflection coefficients of a wave p_1^+ measured for $p_2^-=0$. This condition is achieved for a sound source placed upstream and an anechoic termination placed downstream of the discontinuity. The elements t^- and r^- are the equivalent transmission and reflection coefficients of a p_2^- wave measured when $p_1^+=0$.

Frequencies such that only plane acoustic waves propagate in the pipe segments are considered. The highest frequencies considered are about one tenth of the cut-off frequency for propagation of higher order acoustic modes. Far from any discontinuities, this implies that the acoustic pressure $p'(x)$ is given by

$$p_i'=p_i^+ \exp[-ik_i^+x]+p_i^- \exp[ik_i^-x] \tag{2}$$

with $i=1,2$. The frequencies considered are so high that visco-thermal dissipation can be described in terms of a small correction to the wave numbers:

$$k^\pm=\frac{\omega}{c_i\pm u_i}+(1-i)\alpha_i^\pm, \tag{3}$$

where $\alpha_i^\pm$ is the damping coefficient and u_i the mean velocity of the flow. Complex wave numbers k_i^+ and k_i^- are given in the Appendix.

When calculating the velocity perturbations u' due to the acoustic waves we neglect the effect of friction:

$$u_i'=\frac{p_i^+-p_i^-}{\rho_i c_i} \tag{4}$$

while the density fluctuations ρ' are related to the pressure fluctuation by using the equation of state:

$$c_i^2\rho_i' = p_i' + \sigma_i', \tag{5}$$

where σ' are the entropy waves introduced by Ronneberger.[3] Note that $\sigma_1' = 0$ in our applications.

B. Steady flow through an orifice

Consider now a steady flow through an orifice as sketched in Fig. 1. The flow is assumed from the upstream region (1) until the vena contracta (j) of the free jet to be homentropic and frictionless. Furthermore the turbulent mixing region is assumed between the vena contracta (j) and the downstream region (2), to be adiabatic and we neglect wall friction in this region. Using a one-dimensional flow approximation we derive from the integral mass conservation law, the equations

$$\rho_1 u_1 = \rho_2 u_2 \tag{6}$$

and

$$\rho_1 u_1 = \Gamma_0 \frac{S_d}{S_p} \rho_j u_j \tag{7}$$

with $\Gamma_0 = S_j/S_d$. As the flow is adiabatic the total enthalpy is conserved. Assuming an ideal gas with constant γ we have

$$\frac{1}{2}u_1^2 + \frac{\gamma}{(\gamma-1)}\frac{p_1}{\rho_1} = \frac{1}{2}u_2^2 + \frac{\gamma}{(\gamma-1)}\frac{p_2}{\rho_2} \tag{8}$$

and

$$\frac{1}{2}u_1^2 + \frac{\gamma}{(\gamma-1)}\frac{p_1}{\rho_1} = \frac{1}{2}u_j^2 + \frac{\gamma}{(\gamma-1)}\frac{p_j}{\rho_j}. \tag{9}$$

The momentum conservation applied to the mixing region yields

$$p_j + \Gamma_0 \frac{S_d}{S_p}\rho_j u_j^2 = p_2 + \rho_2 u_2^2. \tag{10}$$

This system of equation is complemented by the isentropic flow condition in the jet

$$(p_j/p_1) = (\rho_j/\rho_1)^\gamma. \tag{11}$$

The flow is determined when four variables are specified by boundary conditions. One of these boundary conditions is that the upstream flow is assumed to be homentropic. The numerical procedure for solving this set of equation involves an iterative procedure for which a Newton method is used. In this iterative procedure we take into account the fact that the vena contracta factor Γ_0 depends on the Mach number.

C. Linear perturbation of the flow

We introduce small perturbations p_i', ρ_i', and u_i' of the stationary flow state p_i, ρ_i, and u_i (with $i=1$, 2 or j at the upstream, downstream side or at the jet). The time dependence of the vena contracta factor Γ_0 which is induced by fluctuations in the Mach number is neglected. The linear perturbation of the mass balance equations (6) and (7) yields

$$\frac{1}{c_1}[p_1^+(1+M_1) - p_1^-(1-M_1)] = \frac{1}{c_2}[p_2^+(1+M_2) - p_2^-(1-M_2) + \sigma_2' M_2] \tag{12}$$

and

$$\frac{1}{c_1}[p_1^+(1+M_1) - p_1^-(1-M_1)] = \frac{\Gamma_0}{c_j}\frac{S_d}{S_p}[p_j' M_j + u_j' \rho_j c_j], \tag{13}$$

where the ideal gas law is used to calculate the speed of sound $c_i^2 = \gamma p_i/\rho_i$. The conservation of total enthalpy (8) and (9) can be written in terms of linear perturbations as

$$\frac{1}{\rho_1}[p_1^+(1+M_1) + p_1^-(1-M_1)] = \frac{1}{\rho_2}\left[p_2^+(1+M_2) + p_2^-(1-M_2) - \frac{\sigma_2'}{\gamma-1}\right] \tag{14}$$

and

$$\frac{1}{\rho_1}[p_1^+(1+M_1) + p_1^-(1-M_1)] = \frac{1}{\rho_j}[p_j' + u_j' \rho_j c_j M_j]. \tag{15}$$

The momentum conservation low (10) in terms of linear perturbations becomes

$$\left[p_j'\left(1 + \Gamma_0 \frac{S_d}{S_p} M_j^2\right) + 2u_j' \Gamma_0 \frac{S_d}{S_p}\rho_j c_j M_j\right] = p_2^+(1+M_2)^2 + p_2^-(1-M_2)^2 + \sigma_2' M_2^2. \tag{16}$$

For given incident waves p_1^+ and p_2^-, this set of equations can be solved for the unknowns p_1^-, p_2^+, σ_2', p_j', and u_j'. In principle, the elements t^+, r^+, t^-, and r^- of the scattering matrix of Eq. (1) can be deduced from these results. Explicit expressions are so complex that they do not provide much insight and are therefore not presented.

D. Vena contracta factor

In the present section we provide information on the dependence of the vena contracta factor $\Gamma_0 = S_j/S_d$ on the Mach number M_1, the ratio S_d/S_p of orifice to pipe cross sectional areas, the Reynolds number and the geometry.

As starting point of the discussion, we assume that the orifice has sharp edges and that the Reynolds number is high so that the effect of S_d/S_p and M_1 are mainly considered. Some insight on the influence of the geometry are provided by considering both the slit and the circular orifice. Our analysis is based on the theory for an orifice in which the opening has been replaced by a thin walled pipe of cross section S_d. This corresponds to a Borda tube confined in a pipe of section S_p as shown in Fig. 2.

Using a theoretical approach similar to that of Sec. I B we have the following equation:

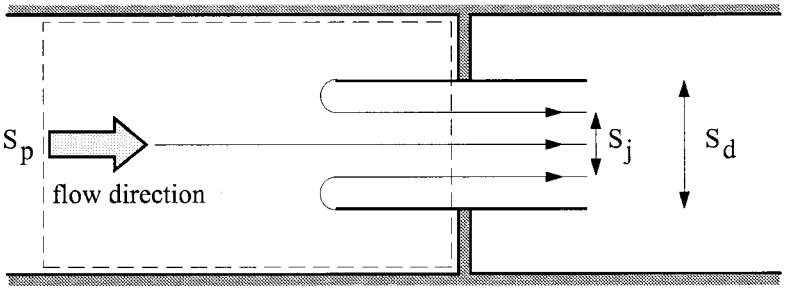

FIG. 2. Confined Borda tube used to derived a theory of the dependence of the vena contracta factor on the Mach number M_1 and the confinement ratio S_d/S_p.

$$\rho_1 u_1 = \Gamma_0 \frac{S_d}{S_p} \rho_j u_j \tag{17}$$

from the mass conservation law, and the equation

$$S_p(p_1 + \rho_1 u_1^2) = (S_p - S_d)p_0 + S_d(p_j + \Gamma_0 \rho_j u_j^2) \tag{18}$$

from the integral momentum equation applied on a control volume enclosing the orifice (see Fig. 2). In this equation the pressure p_0 is the pressure on the upstream side of the orifice plate which is assumed to be uniform and equal to the stagnation pressure of the upstream flow:

$$p_0 = p_1 \left(1 + \frac{\gamma - 1}{2} M_1^2 \right)^{\gamma/(\gamma-1)}. \tag{19}$$

As we assume an homentropic flow down to the vena contracta, we have also the isentropic flow condition (11)

$$p_j / p_1 = (\rho_j / \rho_1)^{\gamma}. \tag{20}$$

Using Eqs. (11), (17), and (18) p_j, ρ_j, and u_j are eliminated to obtain an expression relating Γ_0 to M_1 and S_d/S_p. It is however more convenient to use the jet Mach number $M_j = u_j/c_j$ as a parameter. The jet Mach number M_j is related to the upstream Mach number M_1 by the relationship

$$1 + \gamma M_1^2 = \left(1 - \frac{S_d}{S_p} \right) \left(1 + \frac{\gamma - 1}{2} M_1^2 \right)^{\gamma/(\gamma-1)} + \frac{S_d}{S_p} \left(\frac{1 + \frac{\gamma - 1}{2} M_1^2}{1 + \frac{\gamma - 1}{2} M_j^2} \right)^{\gamma/(\gamma-1)} + \gamma M_j M_1 \left(\frac{1 + \frac{\gamma - 1}{2} M_1^2}{1 + \frac{\gamma - 1}{2} M_j^2} \right)^{1/2}. \tag{21}$$

Once M_j has been determined for given M_1 and S_d/S_p the vena contracta factor is easily calculated from

$$\Gamma_0 = \frac{S_0}{S_d} \frac{M_1}{M_j} \left(\frac{1 + \frac{\gamma - 1}{2} M_j^2}{1 + \frac{\gamma - 1}{2} M_1^2} \right)^{(\gamma+1)/2(\gamma-1)}. \tag{22}$$

For $S_d/S_p < 0.6$ Hofmans[10] found that this formula can be approximated by

$$\Gamma_0 \simeq \frac{1}{1 + \sqrt{1 - (S_d/S_p)}} + \frac{\left(1 + \frac{\gamma - 1}{2} M_j^2 \right)^{\gamma/(\gamma-1)} - 1}{\gamma M_j^2} - \frac{1}{2} \tag{23}$$

which corresponds to an extrapolation formula

$$\Gamma_0(S_d/S_p, M_j) \simeq \Gamma_0(S_d/S_p, 0) + \Gamma_0(0, M_j) - \Gamma_0(0,0) \tag{24}$$

which is assumed to be valid for any orifice. We therefore discuss further the limiting values $\Gamma_0(0,0)$, $\Gamma_0(0,M_j)$, and $\Gamma_0(S_d/S_p,0)$ for both the slit and the circular orifice. For further reference note that the vena contracta factor of a Borda tube in an infinite baffle is in the incompressible limit $\Gamma_0(0,0) = \frac{1}{2}$.

The vena contracta factor of a slit in an infinite baffle can easily be calculated for an incompressible flow ($M_j = 0$) by means of the hodograph method.[14] One finds $\Gamma_0(0,0) = \pi/(2+\pi) \simeq 0.61$. The same value is often quoted for circular diaphragms but the theory predicts following Gilbarg[14] $\Gamma_0 = 0.58$. This discrepancy between the commonly reported vena contracta factor and the theory is expected to be due to Reynolds number effects in the experiments. Some information about Reynolds number dependence has been correlated by Blevins,[15] but we further ignore this effect. Higher vena contracta factors can also be due to the lack of sharpness of the edges of the orifice. An edge radius r to orifice diameter D of $r/D = 10^{-2}$ already explains the difference between experiment and theory.[15]

For a slit using the hodograph method, Busemann[16] found the implicit solution

$$\Gamma_0\left(\frac{S_d}{S_p}, 0 \right) = \frac{\pi}{\pi + 2\left(\frac{1}{\Gamma_0} \frac{S_p}{S_d} - \Gamma_0 \frac{S_d}{S_p} \right) \arctan\left[\Gamma_0 \frac{S_d}{S_p} \right]}. \tag{25}$$

For a circular orifice Idelchik[17] proposes the use of the equation

$$\Gamma_0\left(\frac{S_d}{S_p}, 0 \right) = \frac{1}{1 + \sqrt{0.5(1 - (S_d/S_p))}} \tag{26}$$

which provides in the range $0.1 \leqslant S_d/S_p \leqslant 0.7$ a good fit to the experimental data collected by Gilbarg.[14] For $\Gamma_0(0,0)$, this formula yields the value 0.586 which is the theoretical value obtained by Gilbarg[14] with a simplified theory. The formula for $\Gamma_0(S_d/S_p,0)$ has also a structure similar to the structure which was obtained for the Borda tube in Eq. (23). Also the value $\Gamma_0(S_d/S_p,0) - \Gamma_0(0,0)$ obtained with the for-

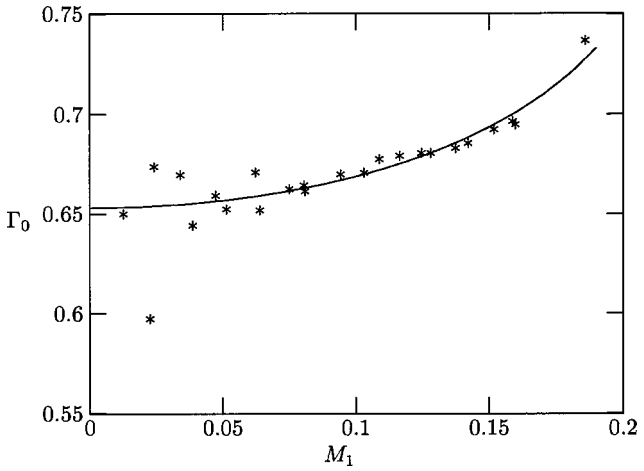

FIG. 3. Vena contracta coefficient Γ_0 of a slit with respect to M_1. *, measurements; —, relation 24 using formula 25 for the term $\Gamma_0(S_d/S_p,0)$ and formula 27 for the term $\Gamma_0(0,M_j)-\Gamma_0(0,0)$. The slit has a height of 10.8 mm and a width of 30 mm. The circular pipe has a diameter of 30 mm.

mula of Idelchik[17] is a good fit of the result of Busemann[16] in the range $0<S_d/S_p\leqslant 0.7$.

The Mach number dependence $\Gamma_0(0,M_j)-\Gamma(0,0)$ appears also to be quite insensitive to the geometry. For a slit Busemann[16,18] proposes an analytical expression based on a simplified model for the gas compressibility. While quite elegant this simplified theory is not very accurate. The value of $\Gamma(0,M_j)-\Gamma(0,0)$ obtained with the Borda tube model [Eq. (23)] appears to be a good fit of the experimental data for a circular orifice reported by Shapiro[18] and the two-dimensional theory without approximation for the gas compressibility. We propose to use the fit formula of Shapiro's solution:

$$\Gamma_0(0,M_j)-\Gamma_0(0,0)=0.13M_j^2 \tag{27}$$

which is a good fit to the theory up to $M_j=0.9$.

In Fig. 3 experimental data obtained with a slit shaped orifice in a circular pipe are compared with the proposed theory. The vena contracta factor has been derived from total pressure losses Δp_t using the Borda–Carnot formula $\Gamma_0=1/[1-\sqrt{(\Delta p_t/p_0)}]$ where p_0 is the upstream stagnation pressure.

For further reference the vena contracta factors measured for a perforated plate and a single orifice with the same (total) value of S_d/S_p are compared in Fig. 4. The perforated plate has 45 holes. We observe that the vena contracta factor of the perforated plate is higher than that of the orifice with a single hole. The difference can be due to the influence of the Reynolds number or to the difference in relative sharpness r/D of the edges of the perforations. Following Blevins,[15] a value $r/D=0.05$ is sufficient to explain this effect. This corresponds to $r=0.175$ mm in the case of the perforated plate. This stresses the importance of accurate geometry of the test elements whereas theoretical works on industrial devices must be based on measured pressure losses coefficients.

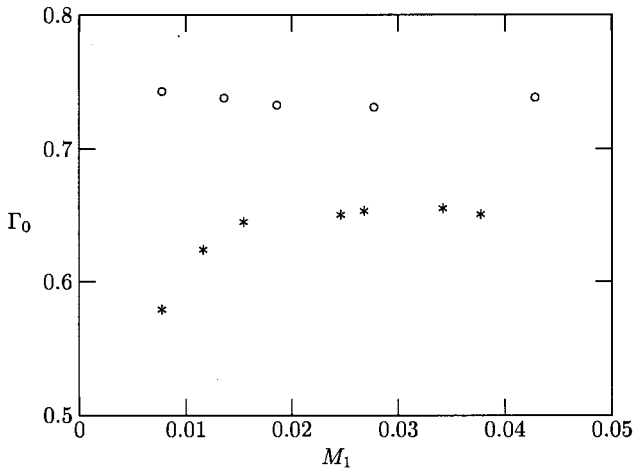

FIG. 4. Vena contracta coefficient Γ_0 with respect to M_1. Comparison between the vena contracta of a single hole orifice and a perforated plate of the same open area ratio. *, round edged single hole orifice inserted in a pipe; ○, perforated plate inserted in a pipe. The single hole orifice diameter is 23.3 mm, the plate is made of 45 holes of diameter 3.5 mm and the pipe diameter is 47 mm. The open area ratio is then 25%.

III. EXPERIMENTAL SET-UPS

A. Measurement method

The reflection coefficient data presented have been obtained by means of the two-microphone method.[19] The scattering matrix data was obtained by means of the two-load method at the TUE and TA-HGE while the two-source method was used at the LAUM. In the scattering matrix experiments two sets of microphones are placed at x_{11} and x_{12} upstream of the discontinuity and at x_{21} and x_{22} downstream of the discontinuity. At each side of the discontinuity the acoustic field is described by Eq. (2). The reflection coefficient R_i follows from the measurement of the transfer function $(H_{21})_i=p_i'(x_{i2})/p_i'(x_{i1})$:[19]

$$R_i=\frac{p_i^-}{p_i^+}=\frac{(H_{21})_i\exp[-ik_i^+x_{i1}]-\exp[-ik_i^+x_{i2}]}{-(H_{21})_i\exp[ik_i^-x_{i1}]+\exp[ik_i^-x_{i2}]}. \tag{28}$$

Note that we have chosen the origin $x=0$ at the discontinuity which we are characterizing. When the reflection coefficient has an absolute value close to unity, which corresponds to a standing wave pattern, the equation becomes singular when $|(x_{i2}-x_{i2})\omega/c_i|=n\pi$ with $n=1,2,\ldots$. Furthermore, as shown by Åbom and Bodén,[19] the accuracy of the measurement decreases strongly when $|(x_{i2}-x_{i2})\omega/c_i|>\pi/2$. This limits the frequency range in which we can measure. At the TUE, three microphones were used which allows us to check the accuracy of the data. At the LAUM, measurements were performed with anechoic terminations upstream and downstream of the discontinuity which reduces the standing wave pattern and makes measurements less sensitive to errors.

When two microphone pairs are placed at both sides of the discontinuity, the transmission coefficient $T_{21}=p_2^+/p_1^+$ can be in addition to the reflection coefficients R_1 and R_2 determined from

$$T_{21}=\frac{p_2'(x_{21})[\exp(-ik_1^+x_{12})+R_1\exp(ik_1^-x_{12})]}{p_1'(x_{12})[\exp(-ik_2^+x_{21})+R_2\exp(ik_2^-x_{21})]}. \tag{29}$$

When two experiments A and B have been performed for the same mean flow conditions but with different acoustic

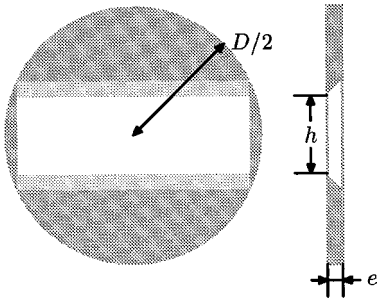

FIG. 5. Sketch of the measured slits. The dimensions are given in Table I.

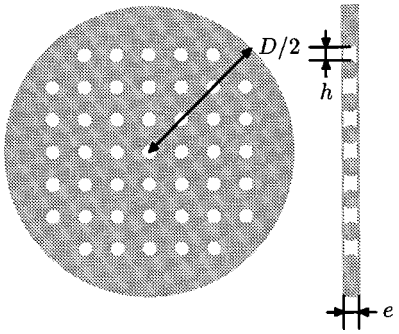

FIG. 6. Sketch of the measured perforated plate. The dimensions are given in Table II.

boundary conditions the scattering matrix is obtained from the set of linear equations

$$T_{21}^{A}=t^{+}+r^{-}R_{2}^{A}T_{21}^{A}, \tag{30}$$

$$R_{1}^{A}=r^{+}+t^{-}R_{2}^{A}T_{21}^{A}, \tag{31}$$

$$T_{21}^{B}=t^{+}+r^{-}R_{2}^{B}T_{21}^{B}, \tag{32}$$

$$R_{1}^{B}=r^{+}+t^{-}R_{2}^{B}T_{21}^{B}. \tag{33}$$

In the case of the two-load method the sound was produced by modulating the main flow by means of a siren (TUE) or a rotating valve (TA-HGE). At the downstream side the setup was terminated by an open pipe end at $x=L$. Two linearly independent experiments were achieved by using two different lengths, respectively $L=L_A$ and $L=L_B$. Optimal conditioning of the experiment is obtained for $|(L_B-L_A)\omega/c_2|=\pi/2$, which corresponds to a quarter wavelength. For $|L_B-L_A|$ equal to a multiple of a half wavelength the method is singular. At the TUE the measurements were restricted to a single optimal frequency. At TA-HGE additional experiments with different length were carried out to extend the frequency range.

When a pipe segment is actually mounted between the two experiments the operation is rather long which requires a corresponding stability of the mean flow conditions. The procedure can be accelerated by using a pipe segment of a quarter wave length placed downstream of a side branch closed by a piston. When the side branch length is increased from zero to a quarter wave length one achieves conditions which are similar to the ones obtained by changing the main pipe length by a quarter wave length. A nice feature of this method is that it can be used at high pressures, replacing the open pipe termination by a vessel with damping material. Drawback of this method is that it is only optimal at a single frequency.

The two-source method removes much of the problems of the two-load method. Loudspeakers were used as sources,[13] one placed upstream and the second placed downstream of the discontinuity. The use of anechoic terminations makes the setup insensitive to frequency. The use of loudspeakers makes it possible to use an automatic source control and therefore to reduce considerably the stability constraint of the main flow by speeding up the measurement procedure.

While the two-source method is more convenient, we did carry out experiments with the two-load method because the use of a siren or a rotating valve allows reproducing flow conditions which are closer to those found in industrial applications such as car mufflers. In particular a siren is a very powerful sound source at low frequencies where a loudspeaker cannot be used.

B. Setups

The technical details of the TUE setup have been provided by Peters.[20] The TA-HGE setup is described in the thesis of Durrieu.[21] The LAUM setup is described in the thesis of Ajello.[13] Some essential differences between the setups are now given.

At the TUE, we focused on the Mach number dependence of the scattering matrix at low frequency and high mass flow and the test of the anechoic termination for combustion experiments. The siren frequency and flow are stable within the experimental accuracy ($\Delta f/f=10^{-4}$, $\Delta M/M=10^{-2}$) during each experiment. A FFT procedure was used with a frequency discretisation corresponding to the experimental accuracy. Measurements were only carried out at the fundamental frequency generated by the siren. The coherence of the signals was larger than 0.999 99 (in most cases at least 0.999 999). The gas temperature T was deduced from the measured wall temperature T_w assuming a recovery factor for a turbulent boundary layer:[18]

$$T_w=T\left(1+\mathrm{Pr}^{1/3}\frac{\gamma-1}{2}M^2\right). \tag{34}$$

The accuracy of this temperature has been estimated to be 0.2 °C. The pipe diameter was $D=3.001$ cm. The test diaphragms used are slit shaped as shown in Fig. 5. The accuracy of the slits geometry was 0.01 mm. Special care

TABLE I. Labeling and dimensions of the orifices measured at the TUE and at the LAUM. The test pipe has a diameter of 30.01 mm.

Label	Width (mm)	Height (mm)	Thickness (mm)	Open area ratio (%)
Large slit (I)	30.01	10.8	4	45.76
Narrow slit (II)	30.01	2.7	4	11.46

TABLE II. Labeling and dimensions of the orifices measured at TA-HGE. The test pipe has a diameter of 47 mm.

Label	Diameter (mm)	Holes number	Thickness (mm)	Open area ratio (%)
Perforated plate	3.5	45	2	24.95
Diaphragm	23.3	1	2	24.6

was take to keep the edges as sharp as possible. The air was dry and dry air properties as reported by Peters[20] were used. The dimensions of the orifices investigated at the TUE are summarized in Table I.

The test section of the setup of the LAUM is the same as that of Eindhoven. The same microphones and signal conditioning is used. The main difference is that the sources (loudspeakers) are driven by a swept (stepwise) sine software procedure of the HP3565s analyzer. Two-hundred frequencies are scanned step by step within a relatively short time. As three microphones are placed on both sides of the discontinuity the air temperature can be determined from acoustical measurements. It is assumed that this temperature remains constant for all measured frequencies during one experiment, which leaves a considerable redundancy in the experimental data. This information is used by means of a least square procedure. Because the air is not dry, the effect of moisture is taken into account as specified by Ajello.[13]

The setup at TA-HGE has a larger diameter of the main pipe $D=4.7$ cm. This allows mounting the 1/2 inch condensator microphones (B&K 4133) flush to the pipe wall. The transfer functions were measured by means of a tracking method (analyzer DIFA DSA 204). The flow noise limited the frequency to the first few harmonics. The accuracy of the geometry of the test objects is of the order of 0.1 mm. Because the edges are not very sharp, the presented theoretical curves are based on measured pressure loss coefficients $C_D=\Delta p_t/p_0$. The focus of this part of the research was the investigation of the difference between single hole orifices and perforated plates as shown in Fig. 6.

The plate thickness is 1.5 mm the perforation diameter is 3.5 mm. Hence the plate remains relatively thin compared to the diameter of the perforations so that turbulent dissipation in the jets occurs downstream of the plate.[17] The dimensions of the orifices investigated at TA-HGE are summarized in Table II.

IV. VALIDATION OF THE THEORY

The Mach number dependent measurements performed on slits were carried out at the TUE. Figure 7 shows the modulus of the scattering matrix coefficients t^+, r^-, r^+, and t^- of a narrow and a large slit whose open area ratio are 11% and 46%, respectively. The measurement frequency was 77 Hz which is the optimum frequency for the two-microphone when considering the setup arrangement as described in the preceding section. The measurements are compared to three different theoretical predictions. An incompressible theory has been derived by Ajello.[13] The terms of the order of M^2 have been discarded and consequently the term accounting for the fluctuation of entropy is dropped since it is proportional to the square of the Mach number. Two compressible theories are distinguished. Both are derived by using the linearized compressible conservation equations written in Sec. II C: one approach considers a constant vena contracta factor while the second uses the relation (27). The value for the vena contracta coefficient at Mach 0 has been calculated by using the relation (25) a correction being made to account for the geometry of the tested element because relation (25) is valid for a two-dimensional slit. Hence Γ_0 has been calculated by integrating the relation (25) for a pipe diameter varying from h to D. The calculation leads to a value for Γ_0 of 0.653 for the large slit which seems coherent with the experimental data shown in Fig. 3. Note that the value predicted by the relation (26) is 0.658 which is close to 0.653 whereas relation (26) does not take into account the object geometry but only the open area ratio. The value of the vena contracta coefficient is 0.618 for the narrow slit.

As emphasized by the flow dependent theories, matrix coefficients depend strongly on the Mach number. This is all the more the case as the slit open area ratio decreases. The compressibility is expected to have an important influence for a Mach number in the jet above 0.3. Indeed the incompressible and compressible theoretical behaviors start to diverge for a Mach number of about 0.08 for the large slit and at about 0.02 for the narrow slit. Next the relevance of using a compressible vena contracta coefficient seems to be confirmed by the measurements of the direct coefficients t^+ and r^+ whereas it is less obvious for the reverse coefficients t^- and r^-. The compressible theory with $\Gamma_0(S_d/S_p,M_j)$ is however in all cases better than the compressible theory ignoring the Mach number dependence of the vena contracta coefficient. Moreover it can be concluded that a quasisteady theory predicts well the response of the slits at the frequency of measurements. Significant deviations have been observed by Ronneberger[8] at higher frequencies. Therefore some frequency dependent measurements were carried out in order to check the limit of the validity of the quasisteady modelling. These measurements were performed at the LAUM for frequencies up to 800 Hz.

Figure 8 presents the measured modulus of the scattering matrix coefficients with respect to frequency. The plots emphasize a weak frequency dependence. This tendency which is not explained by a one-dimensional theory has been reported by Ajello[13] for a circular diaphragm and by Ronneberger[3,8] for a perforated plate and at higher Mach numbers. The deviation is more accentuated as the Mach number increases. At high frequencies the distance over which the jet develops is no longer much shorter than the hydrodynamic wavelength: for the conditions of Fig. 8 the Strouhal number $\mathrm{Sr}=fh/u_d$ (where u_d is the mean flow velocity at the orifice) is about 1/4 at 800 Hz. The variation of the coefficients does not exceed 5% on the curves shown and

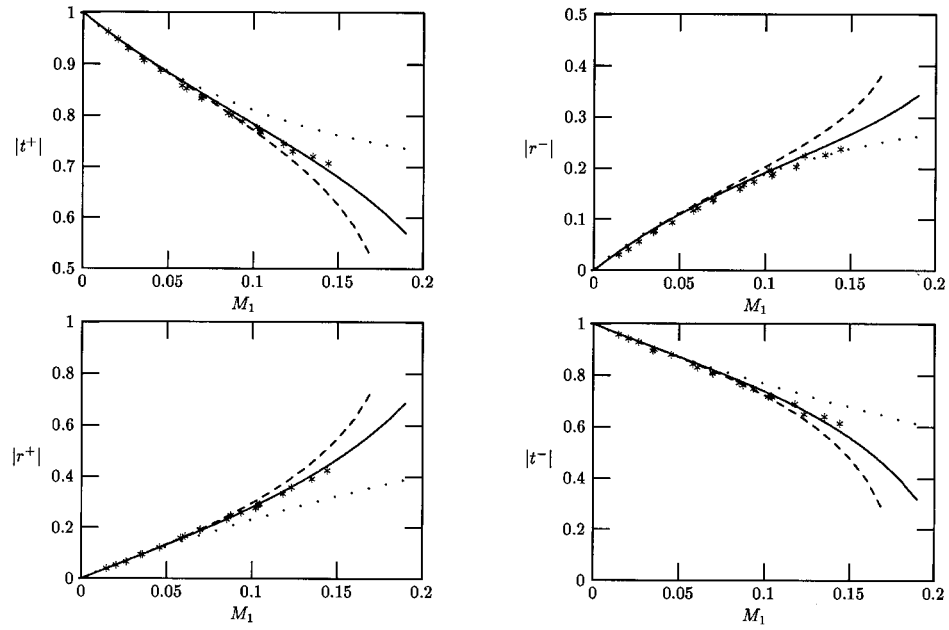

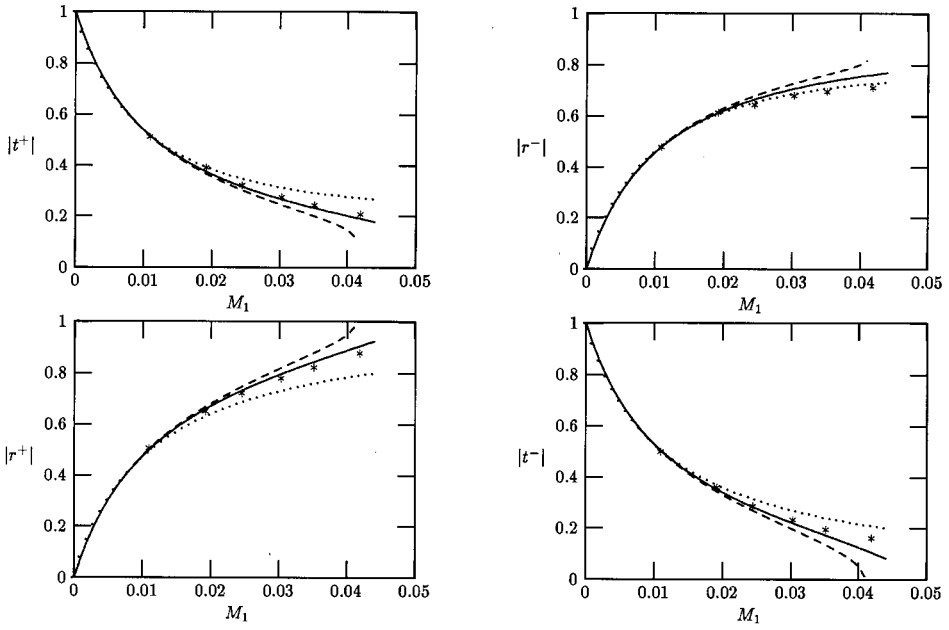

FIG. 7. Modulus of the scattering matrix coefficients with respect to M_1. —: Compressible theory with $\Gamma_0(S_d/S_p, M_j)$; ---, compressible theory with $\Gamma_0(S_d/S_p, 0)$; $\cdots$, incompressible theory. $f = 77$ Hz.

we chose not to investigate this phenomenon giving regard both to its relatively small importance at the frequencies of interest and to the complexity of the existing theories (see the introduction).

Figure 9 presents the argument of the matrix coefficients with respect to M_1 for a frequency of 77 Hz. It is not easy to extract pertinent information from the curves describing the Mach number dependence of the arguments. In particular the variation of the arguments of the reflection coefficients are much weaker than those observed by, e.g., Hofmans[10] and Ronneberger.[8] These variations have been predicted by Hofmans[10] by using a numerical code based on the vortex-blob method. They occur for Sr of the order of 1.0 which is much larger than the Strouhal numbers measured here (in our experiments $0.0008 < \mathrm{Sr} < 0.06$). At Mach 0 the frequency dependence of the argument is well predicted by the addition of an acoustic mass. This is illustrated by Fig. 10 in which are plotted the arguments of the matrix coefficients with respect to frequency for $M_1 = 0$. The theoretical curves shown in Fig. 10 are derived by using the expression of the acoustic mass given by Morse and Ingard[22] and whose length is written as

$$\Delta l = \frac{2h}{\pi} \ln\left(\frac{1}{2} \tan\frac{\pi h}{4D} + \frac{1}{2} \cot\frac{\pi h}{4D} \right). \tag{35}$$

In this case Δl is equal to about 4.3 mm which is almost 2 times larger than the well-known approximation of Fock[23]

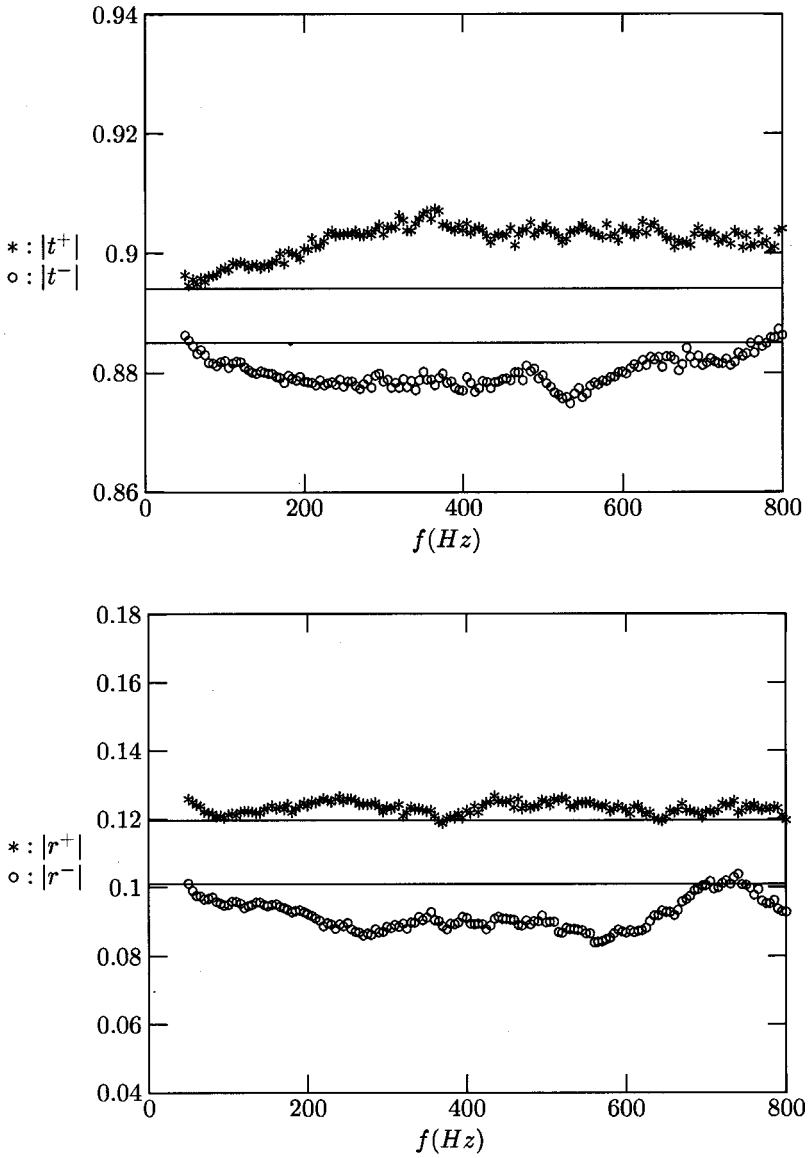

FIG. 8. Modulus of the scattering matrix coefficients of the slit (I) with respect to frequency. ∗, t^+ and r^+; ○, t^- and r^-; —, theoretical predictions. $M_1 = 0.045$.

for the circular diaphragm. This is an illustration of the important geometrical dependence of the acoustic mass (e.g., Refs. 24 and 25). As for the Mach number dependence of the acoustic mass it is emphasized in Fig. 11 which shows the argument of the reflection coefficient with respect to frequency for a Mach number equal to 0.045. Again the theoretical curves are derived by using the expression of Morse and Ingard[22] at Mach 0. These authors suggest that in a presence of flow the acoustic mass is divided by 2. This quantitative assumption is contradicted by our measurements. At high frequencies (200 Hz). it is close to the value at Mach 0. Below 100 Hz, negative values of $\varphi(r^-)$ are observed. A similar complex behavior has been reported by Ajello[13] for circular diaphragms and Peters[20] for open pipe terminations.

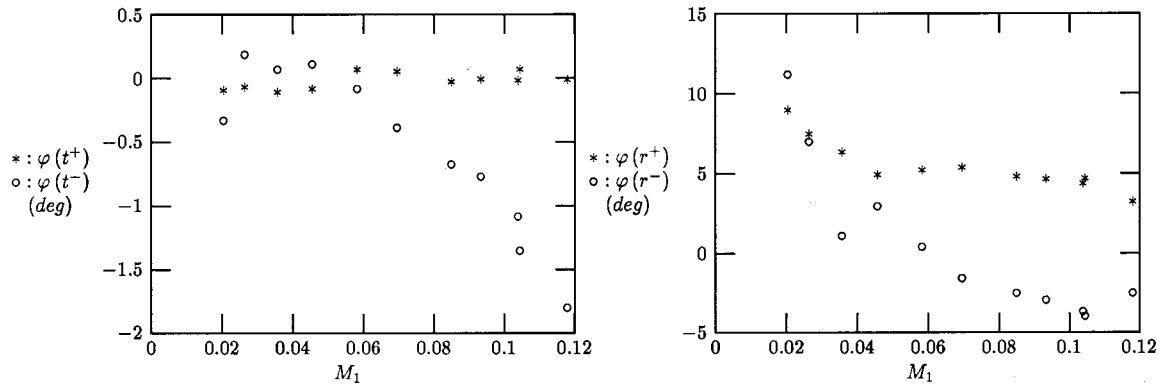

FIG. 9. Argument of the scattering matrix coefficients of the slit (I) with respect to the Mach number. $f = 77$ Hz.

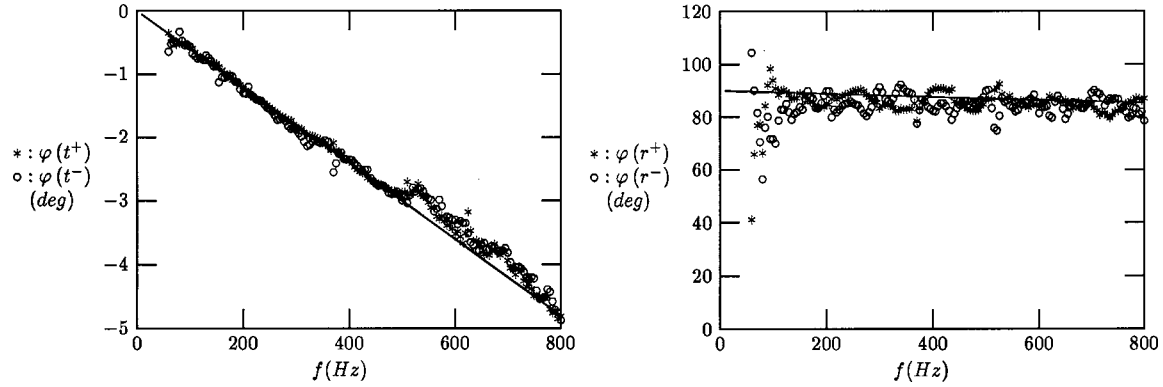

FIG. 10. Argument of the scattering matrix coefficients of the slit (I) with respect to frequency. ∗, ○, measurements; —, theory derived by using the acoustic mass given by Morse and Ingard. $M_1=0$.

Further measurements have been carried out at TA-HGE in order to investigate the behavior of diaphragmlike elements that are commonly used in the design of car silencers. These elements are the rounded edged diaphragm and the perforated plate. Figure 12 presents the comparison of a perforated plate and a rounded edged diaphragm of equal open area ratio of about 25%. The measurements were carried out by using four microphones working in pairs. For each pair the distance between the microphones is about 90 cm so that optimum measurements are obtained for frequencies of 100 Hz, 300 Hz,..., where the points at which the two-microphone method fails have been discarded. Predictions are also shown in the Figure: they are calculated by using a vena contracta coefficient directly extracted from the measured static pressure difference presented in Fig. 4. The frequency dependence of the modulus discussed above is also seen in the Figure, although it is much less clear than in Fig. 8. The interesting feature is that this frequency dependence seems to be weak in the case of the perforated plate. This behavior is also reported by Ronneberger[8] for measurements performed at much higher frequencies. It can be predicted by the addition of an acoustic mass: indeed contrary to the modulus of the circular diaphragm, $|t^+|$ and $|t^-|$ slightly decrease linearly with frequency and $|r^+|$ and $|r^-|$ slightly increase with frequency. This suggests that the frequency and mass flow limits of the validity of a quasisteady modelling of perforates are beyond those existing for a single hole diaphragm. Furthermore the measurements of the static pressure difference of perforated plates that we performed stress a very weak dependence of the vena contracta coefficient on the Mach number.

The arguments of r^+ and t^+ are shown in Fig. 12. For the circular diaphragm we use the approximation calculated by Fock[23] while for the perforated plate we use the expression given by Allard[26] which is written as

$$\Delta l = 0.48 S^{1/2}(1-1.14\Phi^{1/2}), \tag{36}$$

where S is the area of one aperture and Φ is the open area ratio, called porosity in the case of perforates. Due to the measurement accuracy, it is difficult to draw conclusions from the measurements. It seems however that the measured acoustic masses are smaller than those predicted by the acoustic masses, even if, as suggested by Morse and Ingard[22] they are corrected by a factor 2.

V. REFLECTION COEFFICIENT OF A DIAPHRAGM

Diaphragms have been used for many years as devices to reduce low frequency pulsations created, for example, behind compressors. One of the most recent works on this topic is the low frequency nonreflecting endplate presented by Bechert.[6] Bechert studied the sound absorption which occurs at a discontinuity in the presence of flow. For this purpose he derived a simple low frequency model of the flow past an orifice placed at the end of a duct. In this approach, all the kinetic energy is assumed to be absorbed by the turbulence

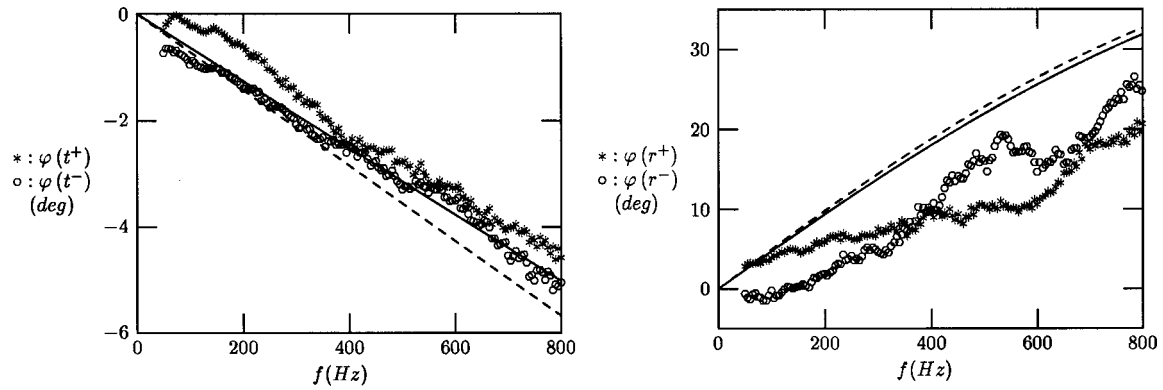

FIG. 11. Argument of the scattering matrix coefficients of the slit (I) with respect to frequency. ∗, t^+ and r^+; ○, t^- and r^-; —, theoretical predictions for t^+ and r^+ using the formula 35; ---, theoretical predictions for t^- and r^- using the formula 35. $M_1=0.045$.

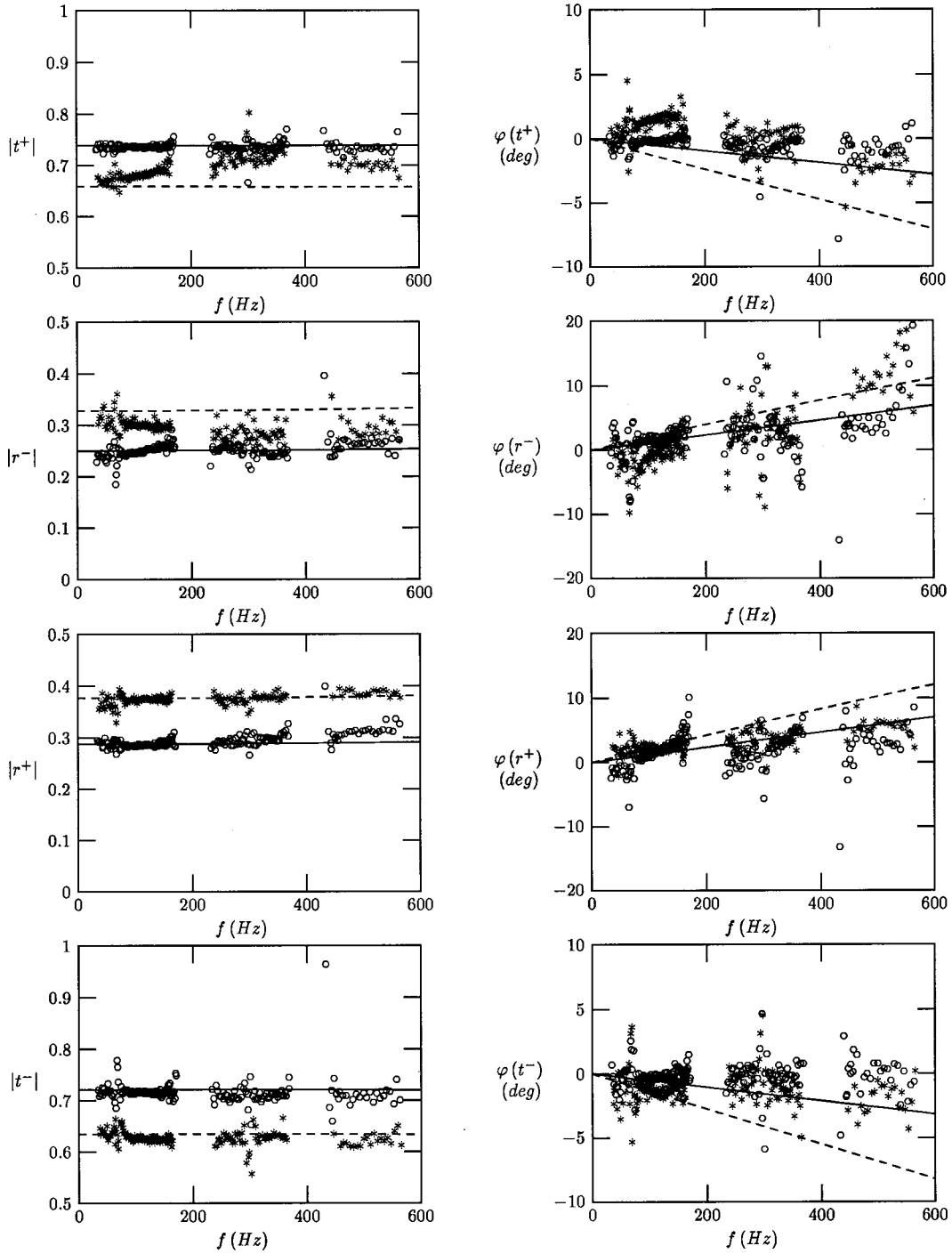

FIG. 12. Modulus and argument of the scattering matrix coefficients of circular orifices of same open area ratio with respect to frequency. ○, perforated plate; *, diaphragm; —, theoretical prediction for the perforated plate; ---, theoretical prediction for the diaphragm. $M_1 = 0.036$. The orifices dimensions are given in Table II.

generated at the edges of the diaphragm. The term $\frac{1}{2}\rho o u_j^2$ disappears in the integral momentum equation derived over the orifice and the pressure in the jet equals the pressure outside. Then if we assumed that the transmitted wave is negligible at low frequencies the reflection coefficient R_1 is expressed by the following relation:

$$R_1 \approx -\frac{1-M_1[(S_p/S_j)^2-1]}{1+M_1[(S_p/S_j)^2-1]}. \tag{37}$$

For an upstream Mach number M_1 equal to $S_j^2/(S_p^2 - S_j^2)$ there is no reflection. For a Mach number belonging to the neighborhood of $S_j^2/(S_p^2-S_j^2)$, the reflection is low but this anechoic region is rather narrow. Only a combination of different open area ratio diaphragms will ensure an effective anechoic termination over a large Mach number range. If we describe the acoustic response of each diaphragm by the scattering matrix relation 1 the upstream reflection coefficient $R_1 = p_1^-/p_1^+$ is given by the following relation:

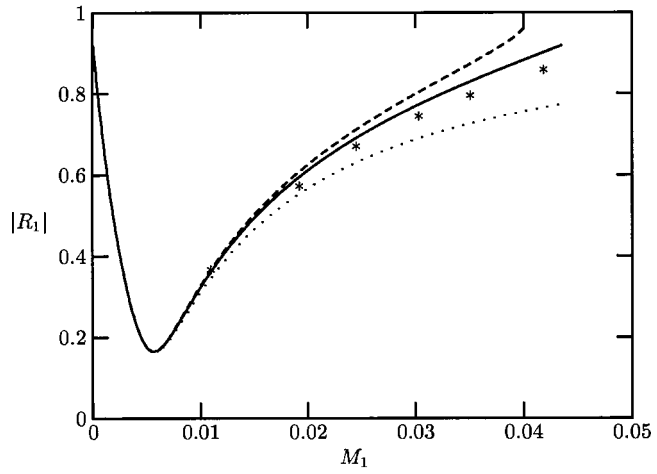

FIG. 13. Modulus of the acoustic reflection coefficient of the slit (II) with respect to M_1. The slit is placed in the pipe at a distance of about 1.8λ from the end pipe, λ being the wave length. *, measurements; —, compressible theory with $\Gamma_0(S_d/S_p, M_j)$; ---, compressible theory with $\Gamma_0(S_d/S_p, 0)$; $\cdots$, incompressible theory. $f=77$ Hz.

$$R_1 = r^+ + \frac{t^+ t^-}{1 - r^- R_2} R_2, \tag{38}$$

with $R_2 = p_2^-/p_2^+$. It is clear that the upstream reflection coefficient depends on the downstream reflection coefficient R_2, that is it depends on the downstream load. For example, if the diaphragm is inserted in an infinite pipe we have $R_1 = r^+$ and this has a minimum only for $S_j^2/(S_p^2 - S_j^2) = 0$. The case of a diaphragm inserted in an open ended pipe is interesting because the reflection coefficient of such a termination, and therefore R_2, is well known.[5,20] This situation is illustrated in Fig. 13 which presents the modulus of R_1 for a slit inserted in a straight pipe at different positions. Both the measurements and the previously discussed theories are shown. The slit is placed in the pipe at a distance of about 1.8λ from the end pipe, λ being the wavelength. $|R_1|$ presents a minimum which is different from zero. The minimum is zero if the downstream pipe length is equal to half the excitation wavelength. Therefore the zero reflection is obtained only at a single frequency. Whatever the diaphragm position is in the pipe the minimum occurs for M_1 close to $1/(S_p/S_j - 1)^2$. This value differs from the one found when the diaphragm is placed at the end of a pipe.

For completeness, note that the compressible expression for the reflection coefficient of a diaphragm placed at the end of a pipe is written as[27]

$$R_1 = -\frac{(1-M_1)[1-(S_p/S_j)^2(\rho_1/\rho_j)^2 M_1]}{(1+M_1)[1+(S_p/S_j)^2(\rho_1/\rho_j)^2 M_1]}. \tag{39}$$

VI. DESIGN OF AN ANECHOIC TERMINATION

Experiments have been carried out at Shell Research (Koninklijke Shell Exploratie en Produktie Laboratorium) on the interaction of combustion and low frequency acoustic pulsations ($1\,\text{Hz} < f < 5\,\text{Hz}$) in long pipe lines. Typical length of the pipes are in full scale a few kilometers. A 1/10 scale model experiment was designed. Obviously pipes of a few hundred meters are still prohibitive in laboratory experiments. We designed mufflers with a length of less than 5 m which mimic reasonably well the almost anechoic behavior of the actual pipe. The use of four to five diaphragms allowed a fair result over a broad frequency range $5\,\text{Hz} < f < 50\,\text{Hz}$ and for a broad range of Mach numbers $0.02 < M < 0.20$. As combustion involves soot formation and large temperatures, it was not possible to use porous media in the damper. The position and dimensions of the orifices was calculated by means of an optimization program using the quasisteady theory. The actual damper performed as predicted. We show here results of comparison of theoretical prediction and measurements carried out at the TUE with an accurately manufactured prototype (see Fig. 14 and Fig. 15). Please note that this prototype was not optimized.

We see that the theory provides a fair prediction of the muffler performances.

VII. CONCLUSIONS

We have presented a quasisteady analysis of the aeroacoustic response of orifices in pipes. Special attention was given to the Mach number dependence and confinement effect on the vena contracta factor both for slits and circular orifices. Experiments with three different setups confirm the significance of Mach number effects. The data for slits and circular orifices has been complemented with results obtained for a perforated plate, which provides information on the influence of the geometry on the response. It appears that only the argument of the scattering matrix parameters is strongly dependent on the geometry. This corresponds to the dependence of the effective mass on the geometry which is well known from the literature in the absence of mean flow. In the presence of mean flow the effective mass of the orifice is not simply half that without flow as suggested by Morse

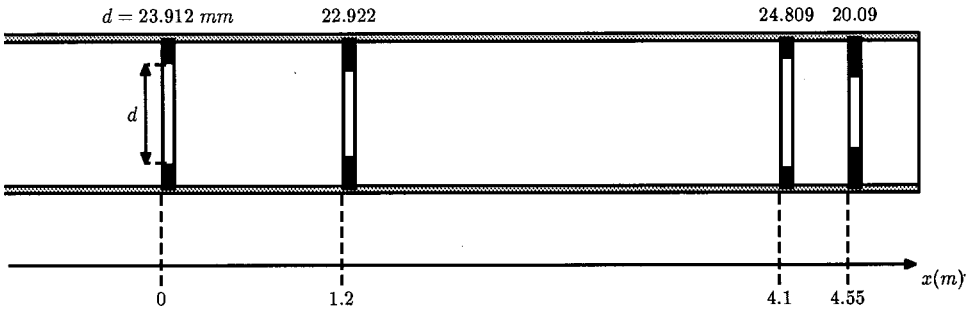

FIG. 14. Geometry of the prototype anechoic termination for combustion experiments in long pipes. The pipe diameter is 30.01 mm.

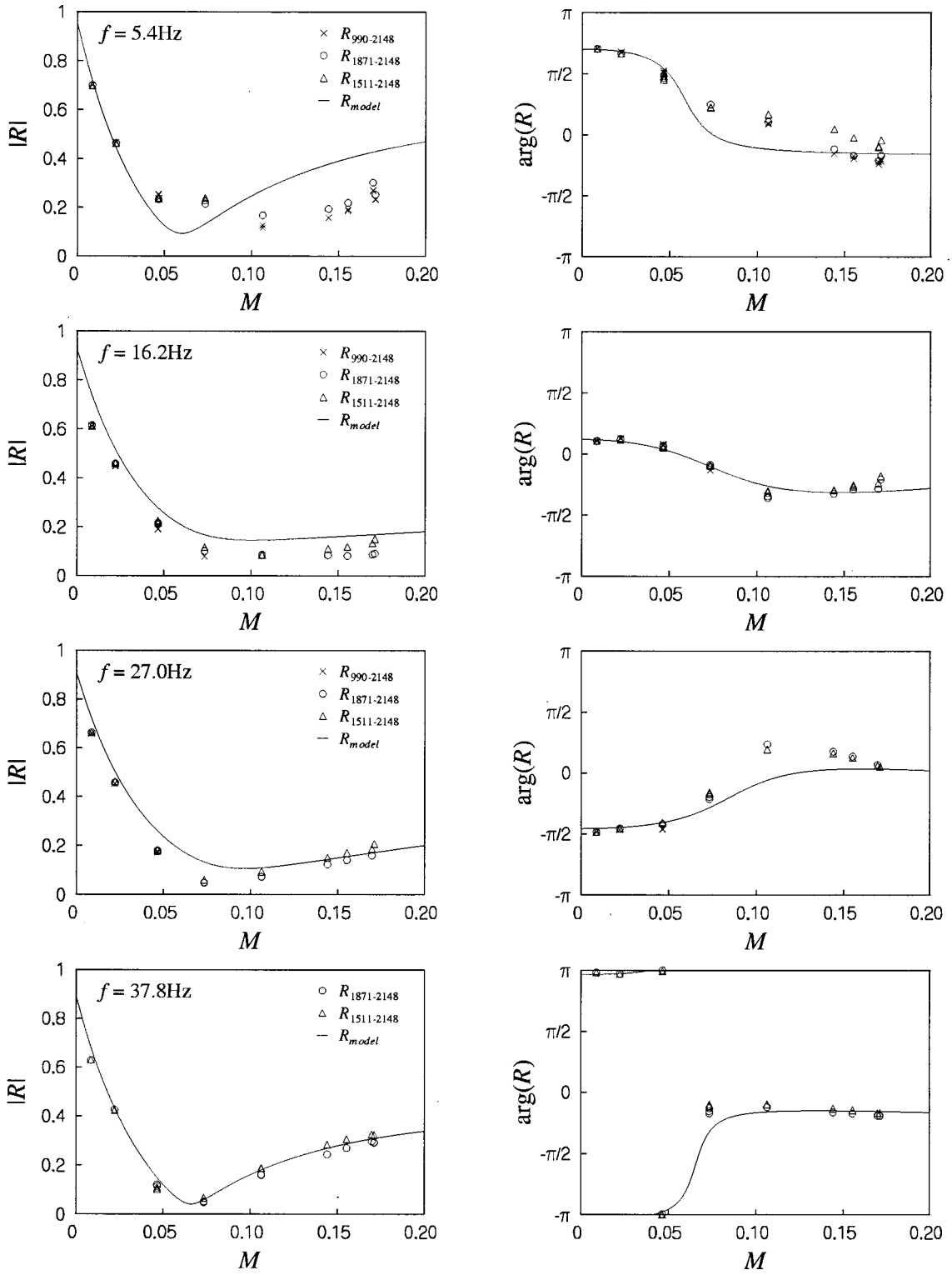

FIG. 15. Comparison of measured Mach number dependence of the reflection coefficient of the anechoic termination with the theory assuming a quasisteady response of the orifices. The different symbols account for different microphones pairs.

and Ingard.[22] A much more complex behavior is observed leading at low frequencies to value lower than half the effective mass without flow. This is analogous to the results obtained by Peters[20] for an open pipe termination. The usefulness of the theory was illustrated by predicting the performance of an anechoic termination consisting of several orifices placed along a pipe.

APPENDIX: VISCO-THERMAL DISSIPATION IN A TURBULENT MAIN FLOW

Complex wave numbers $k^{\pm}$ are given by the following relation:

$$k^{\pm}=\frac{\omega}{c\pm u}+(1-i)\alpha^{\pm}, \tag{A1}$$

where $\alpha^{\pm}$ is the damping coefficient c the speed of sound and u the mean velocity of the flow.

For typical conditions considered here the damping is determined by visco-thermal dissipation in thin boundary layers at the pipe wall. For a kinematic viscosity ν, the value of the damping coefficient is determined by the ratio of the Stokes layer thickness $\delta_{ac}=\sqrt{2\nu/\omega}$ and the thickness δ_l of the viscous sublayer of the turbulent main flow. We use the value of δ_l proposed by Peters:[20]

$$\delta_l = 1.25\nu\sqrt{\rho/\tau_w}, \tag{A2}$$

where ρ is the mean density of the flow and where the wall shear stress τ_w is calculated for a pipe of diameter D by means of the formula of Blasius:[28]

$$\tau_w = \tfrac{1}{8}\psi\rho u^2 \tag{A3}$$

with the friction coefficient ψ given by

$$\psi = 0.3164\left(\frac{\nu}{uD}\right)^{1/4}. \tag{A4}$$

Ronneberger and Ahrens[29] propose a simple model in which the shear waves generated at the wall by the acoustic perturbations are assumed to propagate in the viscous sublayer as in a laminar flow and to reflect on the turbulent core of the flow as if it was a rigid wall. Peters[20] proposes a modification of the rigid core model of Ronneberger and Ahrens[29] by including a phase shift in the reflection of the shear waves which corresponds to the memory of the turbulent flow. In the limit of low Mach numbers $\lim_{M\to 0}\alpha^{\pm}=\alpha$, Peters[20] obtained the formula

$$\frac{\alpha}{\alpha_0} = \frac{1+\exp[-2(1+i)(\delta_l/\delta_{ac})-200i(\delta_l/\delta_{ac})^2]}{1-\exp[-2(1+i)(\delta_l/\delta_{ac})]}, \tag{A5}$$

where α_0 is the damping in a stagnant gas ($M=0$) which is given by Kirchhoff's formula[30]

$$\alpha_0 = \frac{w\delta_{ac}}{cD}\left(1+\frac{\gamma-1}{\sqrt{\mathrm{Pr}}}\right), \tag{A6}$$

where γ is the ratio of specific heats and Pr the Prandtl number. The factor 12.5 in the definition (A2) of δ_l has actually been chosen by Peters[20] in order to obtain a reasonable fit to the experimental data available.[29,20] The correction of the damping coefficient for the influence of convective effects has been successfully predicted by Ronneberger and Ahrens[29] in the case $\delta_{ac}/\delta_l<1$ by means of a ''quasilaminar'' theory. A theory including the influence of turbulence has been proposed by Howe.[31] As such theories are quite complex and we only need the damping as a correction in the interpretation of our experiments, we decide to use the intuitive correction

$$\alpha^{\pm} = \frac{\alpha}{1\pm M}, \tag{A7}$$

where $M=u/c$ is the Mach number.

[1] U. Ingard and H. Ising, ''Acoustic non-linearity of an orifice,'' J. Acoust. Soc. Am. **42**, 6–17 (1967).

[2] A. Cummings and W. Eversman, ''High amplitude acoustic transmission through duct terminations: theory,'' J. Sound Vib. **91**, 503–518 (1983).

[3] D. Ronneberger, ''Experimentelle Untersuchungen zum akustischen Reflexionfaktor von unstetigen Querschnittänderungen in einem luftdurchströmten Rohr,'' Acustica **19**, 222–235 (1967).

[4] D. Ronneberger, ''The acoustical impedance of holes in the wall of flow ducts,'' J. Sound Vib. **24**, 133–150 (1972).

[5] P. O. A. L. Davies, ''Practical flow ducts acoustics,'' J. Sound Vib. **124**, 91–115 (1988).

[6] D. W. Bechert, ''Sound absorption caused by vorticity shedding, demonstrated with a jet flow,'' J. Sound Vib. **70**, 389–405 (1980).

[7] M. S. Howe, ''On the theory of unsteady high Reynolds number flow through a circular aperture,'' Proc. R. Soc. London, Ser. A **366**, 205–223 (1979).

[8] D. Ronneberger, Theoretische und experimentelle Untersuchung Schallausbreichtung durch Querschnittssprünge und Lochplatten in Strömungkanälen, Abschlußbericht zum DFG-Forschungvorhaben Ro 369/11, 12, 14, Drittes Physikalisches Institut, Göttingen, 1987.

[9] I. J. Hugues and A. P. Dowling, ''The absorption of sound by perforated linings,'' J. Fluid Mech. **218**, 205–235 (1990).

[10] G. C. J. Hofmans, ''Vortex sound in confined flows,'' Ph.D. thesis, Eindhoven University of Technology, 1998.

[11] M. Åbom, ''Measurement of the scattering matrix of acoustical two ports,'' Mech. Syst. Signal Process. **5**, 89–104 (1991).

[12] M. L. Munjal and A. G. Doige, ''Theory of a two source-location method for direct experimental evaluation of the four-pole parameters of an aeroacoustic element,'' J. Sound Vib. **141**, 323–333 (1990).

[13] G. Ajello, ''Acoustic measurements in pipe systems with flow: design of a flow bench and applications to measurement of discontinuities,'' Ph.D. thesis, Université du Maine, 1997.

[14] D. Gilbarg, *Encyclopedia of Physics; Volume IX, Fluid Dynamics III. Jets and Cavities* (Springer-Verlag, Berlin, 1960).

[15] R. D. Blevins, *Applied Fluid Dynamics Handbook* (Van Nostrand Reinhold, New York, 1984).

[16] A. Busemann, ''Hodographenmethode der Gasdynamik,'' Z. Angew. Math. Mech. **17**, 73–79 (1937).

[17] I. E. Idelchik, *Handbook of Hydraulic Resistance*, 2nd ed. (Springer-Verlag, Berlin, 1986).

[18] A. H. Shapiro, *The Dynamics and Thermodynamics of Compressible Fluid Flow* (Ronald, New York, 1953), Vol. I.

[19] M. Åbom and H. Bodén, ''Error analysis of two microphone measurements in ducts with flow,'' J. Acoust. Soc. Am. **83**, 2429–2438 (1988).

[20] M. C. A. M. Peters, ''Aeroacoustic sources in internal flows,'' Ph.D. thesis, Eindhoven University of Technology, 1993.

[21] P. Durrieu, ''Development of experimental and predictive tools aimed at investigating the acoustical behaviour of car silencer components,'' Ph.D. thesis, Université du Maine, 1999.

[22] P. M. Morse and K. U. Ingard, *Theoretical Acoustics* (Princeton University Press, Princeton, NJ, 1968).

[23] V. A. Fock, ''A theoretical investigation of the acoustical conductivity of a acoustical conductivity of a circular aperture in a wall put across a tube,'' C. R. (Dokl.) Acad. Sci. URSS **31**, 875–878 (1941).

[24] J. Kergomard and A. Garcia, ''Simple discontinuities in acoustic waveguides at low frequencies: critical analysis and formulae,'' J. Sound Vib. **114**, 465–479 (1987).

[25] C. L. Morfey, ''Acoustic properties of openings at low frequencies,'' J. Sound Vib. **9**, 357–366 (1969).

[26] J. F. Allard, *Propagation of Sound in Porous Media: Modeling Sound Absorbing Materials* (Chapman-Hall, London, 1993).

[27] R. J. J. Boot, ''Aeroacoustic behaviour of diaphragms,'' Master's thesis, Report R-1370-A, Eindhoven University of Technology, 1995.

[28] H. Schlichting, *Boundary-layer Theory*, 7th ed. (McGraw-Hill, New York, 1979).

[29] D. Ronneberger and A. Ahrens, ''Wall shear stress caused by small amplitude perturbations of turbulent boundary layer flow: an experimental investigation,'' J. Fluid Mech. **83**, 433–464 (1977).

[30] A. D. Pierce, *Acoustics: An Introduction to its Physical Principles and Applications* (McGraw-Hill, New York, 1981).

[31] M. S. Howe, ''The damping of sound by wall turbulent shear layers,'' J. Acoust. Soc. Am. **98**, 1723–1730 (1995).